ACS OMEGA

http://pubs.acs.org/journal/acsodf

Article

Comparative Properties of K/NaX and K/NaY from Ultrasound-Assisted Impregnation and Performance in Transesterification of Palm Oil

Siriporn Kosawatthanakun, Chaianun Pansakdanon, Narongrit Sosa, Narong Chanlek, Frank Roessner, Sanchai Prayoonpokarach, and Jatuporn Wittayakun*

Cite This: *ACS Omega* 2022, 7, 9130–9141

Read Online

ACCESS | Metrics & More | Article Recommendations

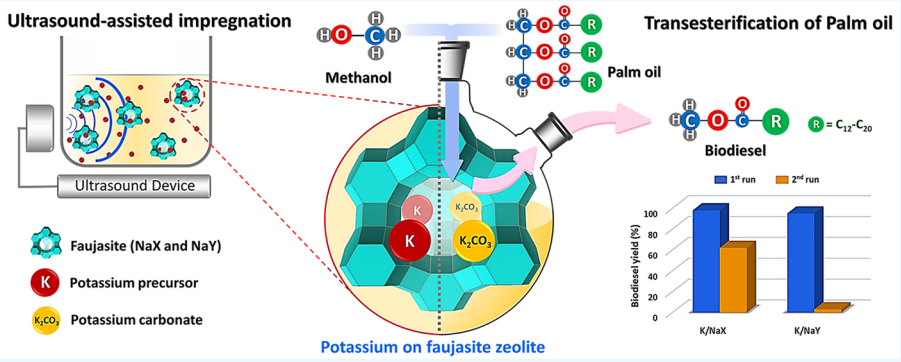

ABSTRACT: This work aims to compare physicochemical properties and catalytic performance of potassium supported on zeolite NaX and NaY (K/NaX and K/NaY, respectively) prepared by ultrasound-assisted impregnation from potassium acetate buffer precursor. Calcination converts the potassium precursor to carbonate, which occupies the zeolite cavities and disperses on the external surface. Both calcined samples show a decrease in zeolite phases, BET surface areas, and pore volumes. With the smaller changes, K/NaX is more stable than K/NaY. Moreover, K/NaX has higher basicity than K/NaY and is more active in the decomposition of 2-methylbut-3-yn-2-ol (MBOH), producing dominant products from basic sites. Both K/NaX and K/NaY are active in the transesterification of palm oil, producing more than 94% of the biodiesel yields in the first run. However, the yields drop in the second run because of the leaching of potassium species into glycerol and biodiesel products. The spent K/NaX has a similar phase to the fresh one, whereas the spent K/NaY shows more structure collapse. With better structural stability, less potassium leaching, and less decline in biodiesel yields in the second run, K/NaX is a better catalyst than K/NaY.

1. INTRODUCTION

Biodiesel is an alternative fuel produced from various renewable feedstocks. The process involves transesterification, a reaction between triglyceride and alcohol (such as methanol) in the presence of a catalyst. One of the most used catalysts is homogeneous alkaline solutions which provide a high product yield. However, a large amount of wastewater is generated from the product purification step. Consequently, there is an increased interest in developing heterogeneous catalysts that are easy to separate from the products and are reusable. Examples of heterogeneous base catalysts for transesterification are carbonates, alkali, metal oxides, and zeolites.[1−3] Those catalysts require a smaller alcohol volume than acid catalysts.[4] Currently, there are several review articles with various aspects in development on heterogeneous catalysis for biodiesel production including current status and challenges;[5,6] evaluation on feedstocks, technologies, catalysts, and reactors;[7,8] advances in reactors;[9] and processing technologies.[10]

One of the promising catalysts consists of potassium (K) species on various supports.[11−13] They have higher basicity and better resistivity to free fatty acids contaminating in triglyceride sources than those with lithium and sodium.[11] They could be reused with fewer activity losses than the other catalysts. Moreover, the dispersion of active species on porous materials could improve the catalyst activity.

Received: September 6, 2021
Accepted: March 2, 2022
Published: March 11, 2022

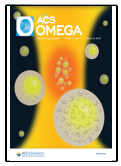

https://doi.org/10.1021/acsomega.1c04912
ACS Omega 2022, 7, 9130−9141

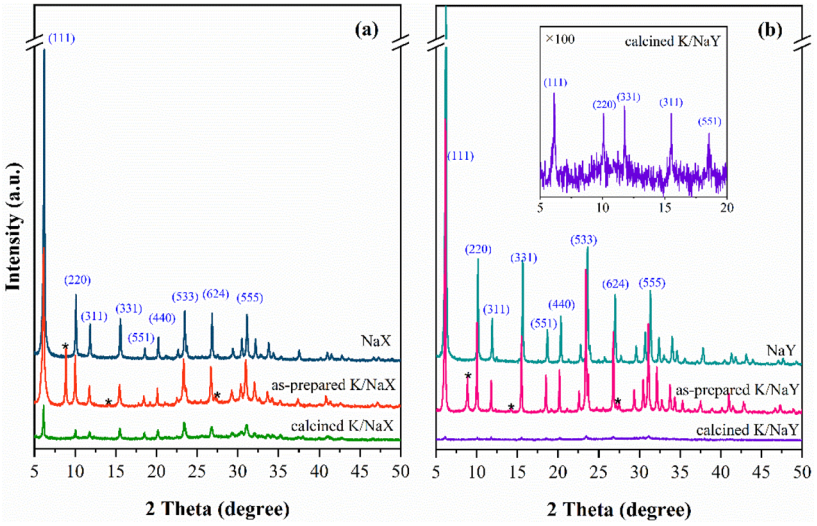

Figure 1. XRD patterns of as-prepared and calcined (a) K/NaX and (b) K/NaY compared with their parent zeolites; symbol (*) = potassium acetate phase.

Among porous materials, zeolites faujasite (FAU) including NaX and NaY are interested in this work. They have well-defined frameworks with a three-dimensional pore system, large surface areas, high ion-exchange abilities, and thermal stability.[14] Moreover, they are commercially available in a large scale. Both NaX and NaY zeolite have the same FAU structure but different Si/Al ratios, namely, 1−1.5 in NaX and >1.5 in NaY. The presence of aluminum in the zeolite structure generates a framework negative charge, which requires extraframework cations for charge balancing.[15,16]

There are several works on catalysts with potassium supported on NaX and NaY for transesterification of various oils from plants such as palm, soybean, sunflower, and jatropha.[12,13,17−19] The catalysts are prepared commonly by impregnation with potassium hydroxide (KOH), potassium nitrate (KNO_3), and potassium acetate buffer (CH_3COOK/CH_3COOH).[12,13,17−22] The basicity increases with potassium loading, resulting in better biodiesel yields. Some of those catalysts have problems from the collapse of the zeolite structure or the agglomeration of potassium species. Moreover, there is not much comparison of catalysts on the same condition or the same oil. The understanding of catalyst properties is crucial to pursue the challenges in catalyst design and development.

Early works focused on the preparation of catalysts that produced high biodiesel yields. Noiroj et al. prepared K/NaY with 10 wt % KOH as an effective catalyst for transesterification of palm oil.[18] Intarapong et al. found that the increase in KOH loading on NaY increased the basicity but destroyed the zeolite structure.[20] Xie et al. reported that K/NaX from 10% KOH was the best catalyst in transesterification of soybean oil. The increase in KOH loading increased basicity but led to the collapse of the zeolite framework and agglomeration of potassium species.[21] Peña et al. demonstrated that K/NaX from KNO_3 gave a high biodiesel yield from transesterification of sunflower oil.[19]

There are some works that concern the stability of zeolite supports. Supamathanon et al.[13] and Manadee et al.[17] prepared K/NaY and K/NaX by impregnating the zeolites with a potassium acetate buffer solution to produce active catalysts for transesterification of Jatropha seed oil. This potassium precursor could minimize the zeolite structure collapse. Both studies showed that the catalysts have smaller surface areas than the parent zeolites after loading with K precursor, probably due to the agglomeration of potassium species. Hence, ultrasound-assisted impregnation was proposed to improve the dispersion.

Ultrasound has been applied to assist material modification and synthesis. The ultrasound causes acoustic cavitation providing the formation, growth, and collapse of hot gas bubbles in a liquid system. The collapsed bubbles then increase the temperature and the pressure, which assists the diffusion of the precursor into support pores and improves surface interaction.[23] There are a few reports on ultrasound-assisted impregnation of metal precursors on FAU zeolite.[12,24] Rakmae et al. used ultrasound-assisted impregnation to prepare 12 wt % potassium on NaY from potassium acetate buffer.[12] The catalyst provided a better biodiesel yield than that from a conventional impregnation. Recently, Ketzer et al. used ultrasound-assisted impregnation to prepare 20% WO_3 on ultrastable zeolite Y (USY) for the production of methyl oleate from oleic acid esterification. The catalyst exhibited a high dispersion of active species with strong interaction over the support and provided a good performance.[24]

Although the previous literature shows that the K/NaX and K/NaY are active for the transesterification of various oils, those catalysts were prepared either by different methods or tested on different oils. In addition, there are no reports about the preparation of K/NaX catalysts by ultrasound-assisted impregnation. Consequently, this work aims to compare the physicochemical properties of K/NaX and K/NaY catalysts prepared similarly by ultrasound-assisted impregnation from a potassium acetate buffer solution and their catalytic performance in the transesterification of palm oil under the same condition. Moreover, the properties of the spent catalysts are compared. The in-depth comparison provides an understanding that would be helpful in catalyst design and development.

2. RESULTS AND DISCUSSION

2.1. Characterization of Potassium Catalysts Impregnated on FAU Zeolite. XRD patterns of parent NaX and

https://doi.org/10.1021/acsomega.1c04912
ACS Omega 2022, 7, 9130−9141

NaY zeolites and as-prepared and calcined K/NaX and K/NaY catalysts are shown in Figure 1. NaX and NaY have similar peak positions (JCPDS No. 38−0237 and 39−1380, respectively) but different intensities because of the different Si/Al ratios. The as-prepared K/NaX and K/NaY show the zeolite characteristic peaks with lower intensities than the bare zeolites. Both samples show additional peaks at 8.88, 14.26, and 27.18°, corresponding to the potassium acetate precursor. The peak at 8.88° of the as-prepared K/NaX sample is stronger than the peak of the zeolite 220 plane. However, the as-prepared K/NaY shows the opposite intensities. The results imply that the potassium acetate precursor covers the external surface of NaX with more extent than that of NaY. After calcination, the peaks of the potassium acetate precursor are not observed from both samples, suggesting complete decomposition. However, the zeolite characteristic peaks from both calcined samples have lower intensities than those of the as-prepared samples. The decreased intensities could be from the partial collapse of the zeolite frameworks by hydrolysis of Si−O−Al bonds.[19] Although K/NaX and K/NaY have the same potassium loading, the calcined K/NaX shows stronger zeolite peaks, suggesting less collapse of the zeolite structure. The XRD results suggest that K/NaX is more stable than K/NaY against the same calcination condition.

The SEM images of calcined K/NaX and K/NaY are compared with the parents NaX and NaY, respectively, in Figure 2. Both NaX and NaY are polycrystals with different morphologies. NaX has round-shaped particles with a diameter of about 1.5 μm. Each particle is a cluster of small crystals with various sizes and thicknesses connecting together. The morphology of K/NaX is similar to the parent zeolite but with the poorer sharpness of crystal edges. Some erosion on the surface is visible in the SEM images. NaY consists of single crystals, either perfect octahedra with a diameter of about 500 nm or imperfect polyhedra with various sizes. There are also clusters of crystals with random patterns. The morphology of the calcined K/NaY is similar to that of the parent NaY. The surface of some crystals also shows signs of erosion.

The N_2 sorption isotherms of the calcined K/NaX and K/NaY are compared with the parent zeolites in Figure 3. All samples have type I isotherms, a characteristic of microporous materials.[25] The adsorbed volumes of K/NaX and K/NaY, surface areas, and pore volumes are smaller than the bare zeolites (see Table 1). The decrease could be from the occupation of the impregnated species in the zeolite cavities, blockage of the zeolite pores, and the collapse of the zeolite structure.[12] K/NaX shows a smaller decrease in the adsorbed volume than K/NaY. The results imply that K/NaX has less potassium species in the zeolite cavities or less pore blocking. However, the XRD results indicate that the collapse of zeolite structure in K/NaX is less than that in K/NaY. Because the hydrolysis of the Si−O−Al bond of zeolites under thermal treatment could be assisted by alkali metal species,[22] the smaller amount of potassium species in the cavities of NaX could be the reason for less collapse. Moreover, the hysteresis loops on NaX and K/NaY are type H4 and H2(b) that could be from crystal aggregation and thermal hydrolysis, respectively.[25]

FTIR spectra and assignment of calcined K/NaX and K/NaY are presented in Figure 4a and Table 2. The peaks at 1388 and 1448 cm^{-1} from K/NaX and 1388 and 1456 cm^{-1} from K/NaY correspond to asymmetric stretching (ν) of carbonate ion (CO_3^{2-}).[17,26] More intense peaks of carbonate are observed on

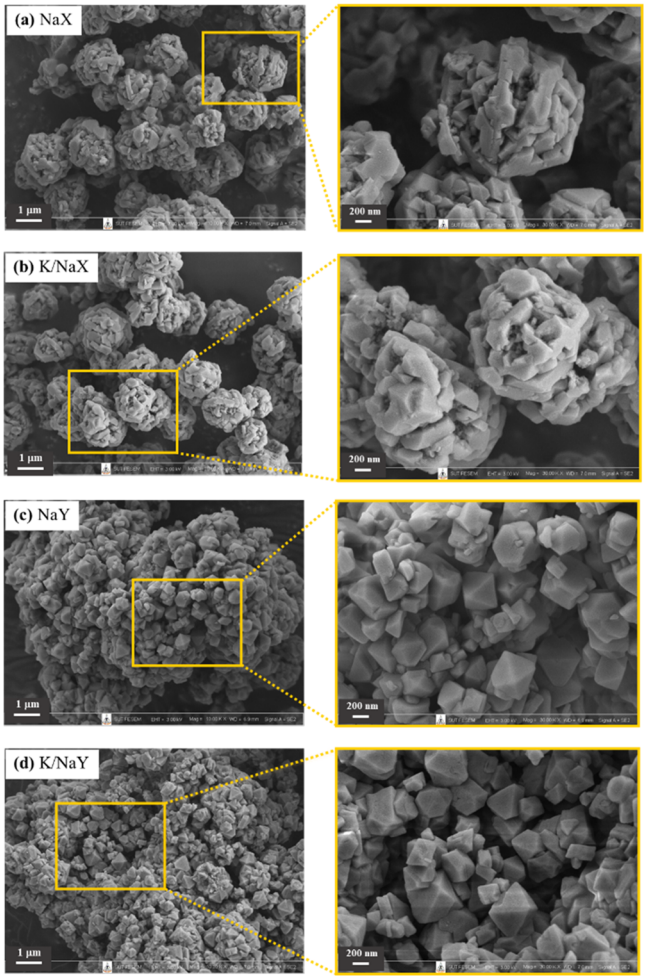

Figure 2. SEM images of (a) NaX, (b) calcined K/NaX, (c) NaY, and (d) calcined K/NaY catalysts with 10k and 30k magnification.

K/NaY, consistent with the stronger potassium acetate peaks in the XRD patterns. Both samples also show a small peak at around 880 cm^{-1}, corresponding to out-of-plane bending (δ) of CO_3^{2-}.[26,27] The bands of stretching and bending of Si−O−T, where T is the Si or Al atom of the zeolites, decrease because of thermal hydrolysis during the decomposition of the acetate precursor.[12] The formation of K_2CO_3 on the support surface may relate to the collapse of the zeolite framework. The finding agrees with the FTIR results in the literature.[12,17]

Raman spectra and peak assignments of both calcined K/NaX and K/NaY are compared with those of the parent zeolites in Figure 4b and Table 2. Both samples show peaks at 1080, 1060, and 700 cm^{-1} corresponding to the stretching and bending modes of K_2CO_3.[28,29] Although both samples were prepared with the same potassium loading, the signal of K_2CO_3 on K/NaX is stronger than that on K/NaY, implying that larger amount of carbonate species is on the external surface.[30] This could also be from the stronger intrinsic basicity of the NaX zeolite. The vibration of 4- and 6-membered rings of FAU frameworks decreased because of hydrolysis during the thermal treatment of the potassium precursor.[12] The relative peak intensity of the 4-membered ring in the NaX framework is higher than that in the NaY. This result confirms that structure of NaX is more stable, consistent with the XRD results.

https://doi.org/10.1021/acsomega.1c04912
ACS Omega 2022, 7, 9130−9141

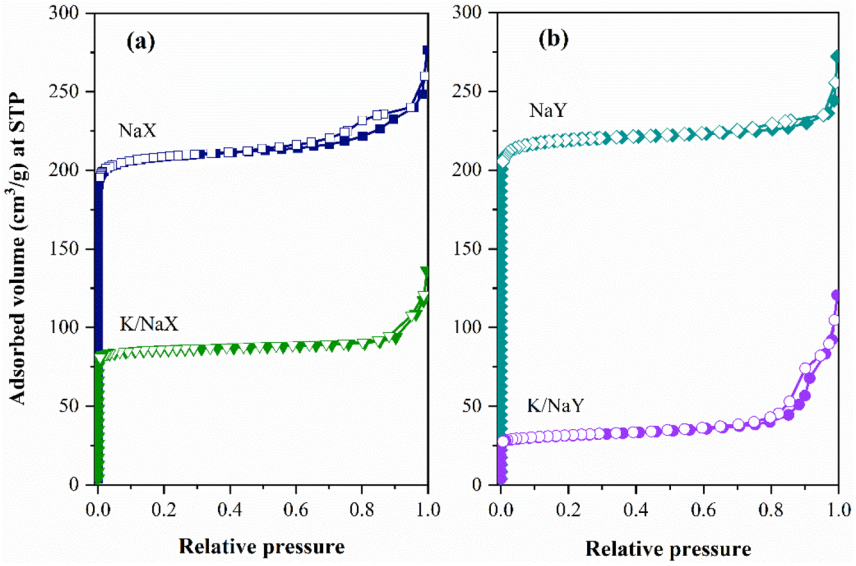

Figure 3. N_2 sorption isotherms of (a) calcined K/NaX and (b) calcined K/NaY compared to their parent zeolites; filled symbols = adsorption and hollow symbols = desorption.

Table 1. BET Surface Area and Micropore Volume of K/NaX and K/NaY Compared to Parent Zeolites from N_2 Sorption Analysis; and K Content from ICP Analysis

sample	BET surface area ($m^2\ g^{-1}$)	micropore volume ($cm^3\ g^{-1}$)	K content (wt %)
NaX	853	0.254	–
NaY	899	0.331	–
K/NaX	352	0.128	11.03 ± 0.07
K/NaY	121	0.037	11.40 ± 0.17

Moreover, the forms of potassium species in calcined K/NaX and K/NaY were determined by XPS. The spectra of K/NaX and K/NaY are shown in Figure 4c. The peaks of K $2p_{1/2}$ and K $2p_{3/2}$ from K/NaX are observed at 295.7 and 293.0 eV, respectively, corresponding to K_2CO_3.[31] Both K 2p peaks from K/NaY shift to lower binding energy, probably due to connection to elements with lower electronegativity.[32] The binding energy difference between K/NaX and K/NaY could be attributed to the interfacial interaction between K species and the zeolite surface. The higher binding energy in K/NaX implies a stronger interaction. The peak at 288.5 eV from both samples corresponds to carbonate species on the zeolite surface. The peaks at 284.6 and 285.9 eV are assigned to adventitious carbonaceous compounds.[12] These XPS results confirm the presence of K_2CO_3 on both zeolites, which are not observed by XRD.

The acid−base properties of the catalysts are distinguished by the decomposition of MBOH.[33] The conversions of MBOH over the calcined K/NaX and K/NaY and the parent zeolites are compared in Figure 5a and Table 3. The conversions from bare zeolites are very low and much lower than K/NaX and K/NaY. These results ensure that the addition of potassium generates more active sites. The conversions from K/NaX are significantly higher than those from K/NaY, indicating the more active sites. These results are consistent with the higher structural stability and larger surface area, which reflects the better dispersion and accessibility of base species in the zeolite cavities. The selectivities of all products are listed in Table 3. NaX provides mainly the base-catalyzed products, whereas NaY produces more compounds formed on coordinatively unsaturated sites. These results indicate that NaX has more basic sites than NaY. After loading with potassium, K/NaX and K/NaY only give the base-catalyzed products. The results confirm that the presence of K_2CO_3 on the zeolite significantly improves the basicity.

CO_2-TPD profiles of calcined K/NaX and K/NaY are shown in Figure 5b, and the calculated values of basicity are listed in Table 3. NaY and NaX show a peak at 300 and 330 °C, respectively. The higher temperature from NaX reflects the stronger intrinsic basicity consistent with a lower Si/Al ratio. After loading with potassium, K/NaX gives a strong peak centered at 680 °C. K/NaY shows peaks in the same temperature range but smaller peak area. This result confirms that K/NaX is more basic than K/NaY. This could be from the better dispersion of base species.[22] The lower basicity in K/NaY is consistent with the result from the MBOH decomposition.

2.2. Catalytic Activity on Transesterification of Palm Oil. Figure 6 displays the GC chromatograms of products from the transesterification of palm oil obtained from the first and second runs on K/NaX and K/NaY. The biodiesel yields from first runs were 97.9 and 94.4%, respectively. Table 4 compares the yields from this work with those from the literature. The biodiesel yield of K/NaY from this work is higher than the work from Rakmae et al.[12] The difference might be from the methods used for product separation; namely, hot filtration in this work versus room-temperature filtration in Rakmae et al.[12] The K/NaX and K/NaY, prepared by the same method, give similar biodiesel yields in the first run despite the more collapse in the zeolite structure in K/NaY. However, the differences are obvious in the second run. From the chromatograms from the second run (Figure 6), the biodiesel yields from K/NaX and K/NaY decreased to 61.3 and 2.7%, respectively. The decrease was mainly due to the leaching of potassium species which is discussed in Section 2.3. This result implies that the amount of K_2CO_3 as a basic site is the key to catalytic activity. Compared to the literature, the performance of K/NaX is better than that of K/NaY, when prepared either from conventional or ultrasound-assisted impregnation.

https://doi.org/10.1021/acsomega.1c04912
ACS Omega 2022, 7, 9130−9141

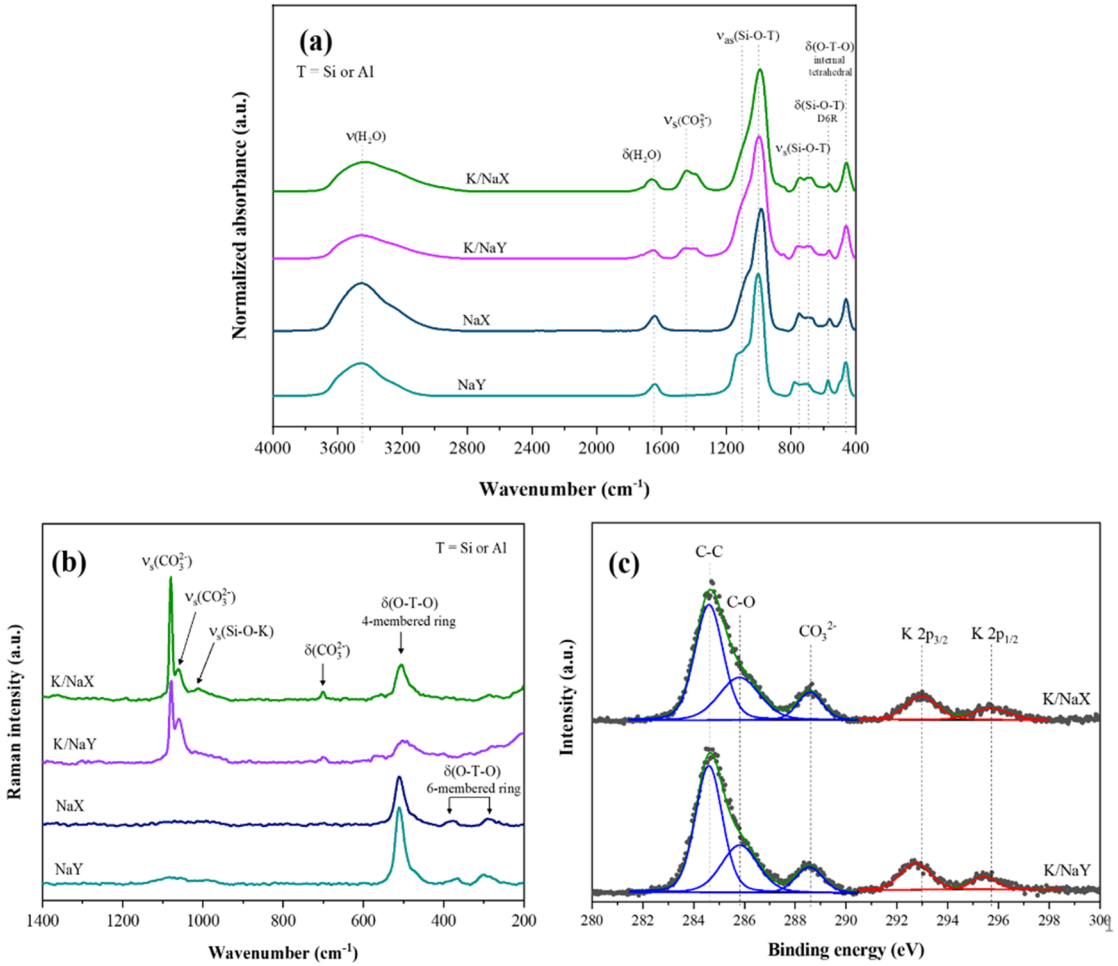

Figure 4. (a) FTIR (KBr method) and (b) Raman spectra of calcined K/NaX and K/NaY catalysts compared with their parent zeolites and (c) XPS spectra of the chemical state of carbon (C 1s) and potassium (K 2p) peaks.

Table 2. Vibration and Peak Assignments of Functional Groups of Samples before and after Calcination

assignment	wavenumber (cm^{-1})						ref
	NaX	as-prepared K/NaX	calcined K/NaX	NaY	as-prepared K/NaY	calcined K/NaY	
Functional Groups Related to Zeolites							
O−T−O bending vibration of S4R (*T* = Si or Al)	458	453	459	463	449	460	34−37
T−O−T bending vibrations of double rings (D6R)	561	563	563	573	569	567	
symmetric stretching of O−T−O	673−748	671−752	679−746	698−779	690−775	685−762	
asymmetric stretching of Si−O−T	984−1069	962	989	1013−1089	978	999	
asymmetric stretching of Si−O−Si (shoulder)	1082	1067	1089	1128	1066	1090	
Functional Groups Related to CH_3COOK							
symmetric stretching of COO^-		1414			1414		38
asymmetric stretching of COO^-		1574			1574		
C−H stretching of $-CH_3$		2977			2980		
Functional Groups Related to K_2CO_3							
symmetric stretching of CO_3^{2-} (ν_1)			1060, 1080			1060, 1080	17,26,27,29
out-of-plane bending of CO_3^{2-} (ν_2)			883			881	
asymmetric stretching of CO_3^{2-} (ν_3)			1448			1456	
in-plane bending of CO_3^{2-} (ν_4)			700			700	
Hydroxyl Regions Related to Zeolites							
symmetric stretching of T−OH	3458	3393	3454	3458	3416	3462	39
in-plane bending of −OH (H_2O)	1641		1659	1641		1653	

https://doi.org/10.1021/acsomega.1c04912
ACS Omega 2022, 7, 9130−9141

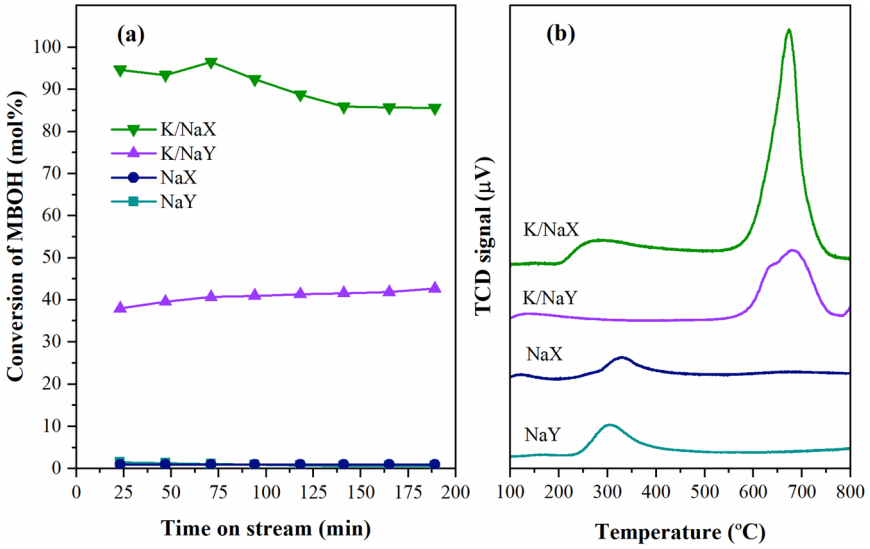

Figure 5. (a) MBOH conversion at various times on stream and (b) CO_2-TPD profiles from calcined K/NaX and K/NaY compared to the bare zeolite supports.

Table 3. Conversion and Selectivity of Products from the Decomposition of MBOH and Basicity by CO_2-TPD of K/NaX and K/NaY Compared to the Parent Zeolites

		product selectivity (mol %)				
		base-catalyzed site		coordinate unsaturated site		
sample	MBOH conversion[a] (mol %)	acetylene	acetone	MBYE	prenal	basicity by CO_2-TPD (mmol CO_2 g^{-1} catalyst)
NaX	0.93	45.35	48.65	6.00	0.00	0.375
NaY	0.69	14.28	17.70	68.00	0.00	0.222
K/NaX	85.90	48.90	51.32	0.00	0.00	0.867
K/NaY	41.61	48.67	51.33	0.00	0.00	0.532

[a]Product selectivity from MBOH decomposition was collected at the time on stream at 140 min after reaching the constant conversion.

2.3. Stability of Catalysts. Although K/NaX and K/NaY give high biodiesel yields in the first run, the yields decrease significantly in the second run. The yield from K/NaX is much higher than that from K/NaY. Thus, further investigation on the catalyst stability was conducted. The amount of potassium leaching into glycerol and biodiesel products was determined by ICP-OES. The spent catalysts were characterized by XRD, SEM, FTIR, and Raman spectroscopy.

The total amount of potassium leaching in the glycerol and biodiesel product from K/NaX and K/NaY are 15.6 and 45.2%, respectively. The results indicate that the catalyst deactivation strongly relates to potassium leaching. Namely, the catalyst with more potassium leaching gives the smaller biodiesel yield in the second run. This finding agrees with the reports by Čapek et al.[40] and Muciño et al.[4] The potassium surface species reacts with glycerol to form a soluble species. The less leaching from K/NaX is consistent with the XPS results in section 2.1. Potassium species in K/NaX has a stronger interaction with the zeolite support.

The XRD patterns of spent K/NaX and K/NaY are compared with the fresh catalysts in Figure 7. The patterns of spent and fresh K/NaX are similar, indicating the zeolite stability against the reaction condition. In contrast, the XRD pattern of spent K/NaY shows characteristic peaks of zeolite NaY on a broad baseline, indicating an amorphous nature. These data confirm the greater collapse of zeolite NaY than that of NaX, consistent with the greater decrease in surface area of K/NaY from the bare zeolite.

The SEM images of the spent K/NaX and K/NaY with 10k and 30k magnification are shown in Figure 8. The images of both spent catalysts are similar to their fresh catalysts. However, the changes in zeolite crystallinity are evident in XRD patterns.

The FTIR-ATR and Raman spectra of spent K/NaX and K/NaY are compared with their fresh catalysts in Figure 9. The IR spectra of both spent catalysts are different from their fresh samples. The carbonate peaks have either lower intensities or different shapes indicating changes after the catalytic test. The changes of the spent catalysts from Raman spectra are more evident than from IR spectra. The decreases in the peaks at 1080 and 1060 cm^{-1} (symmetric stretching) and 700 cm^{-1} (symmetric deformation) agree with the leaching of potassium species. The different shapes of carbonate peaks of spent K/NaX and K/NaY indicate the different interaction.

From this study, both K/NaX and K/NaY deactivate after being tested in transesterification. The causes are the leaching of potassium species, the collapse of the zeolite structure and the changes of carbonate species. However, the contribution of each cause is not clear. Therefore, further investigation is recommended to provide insightful information to improve the catalyst design and development.

https://doi.org/10.1021/acsomega.1c04912
ACS Omega 2022, 7, 9130−9141

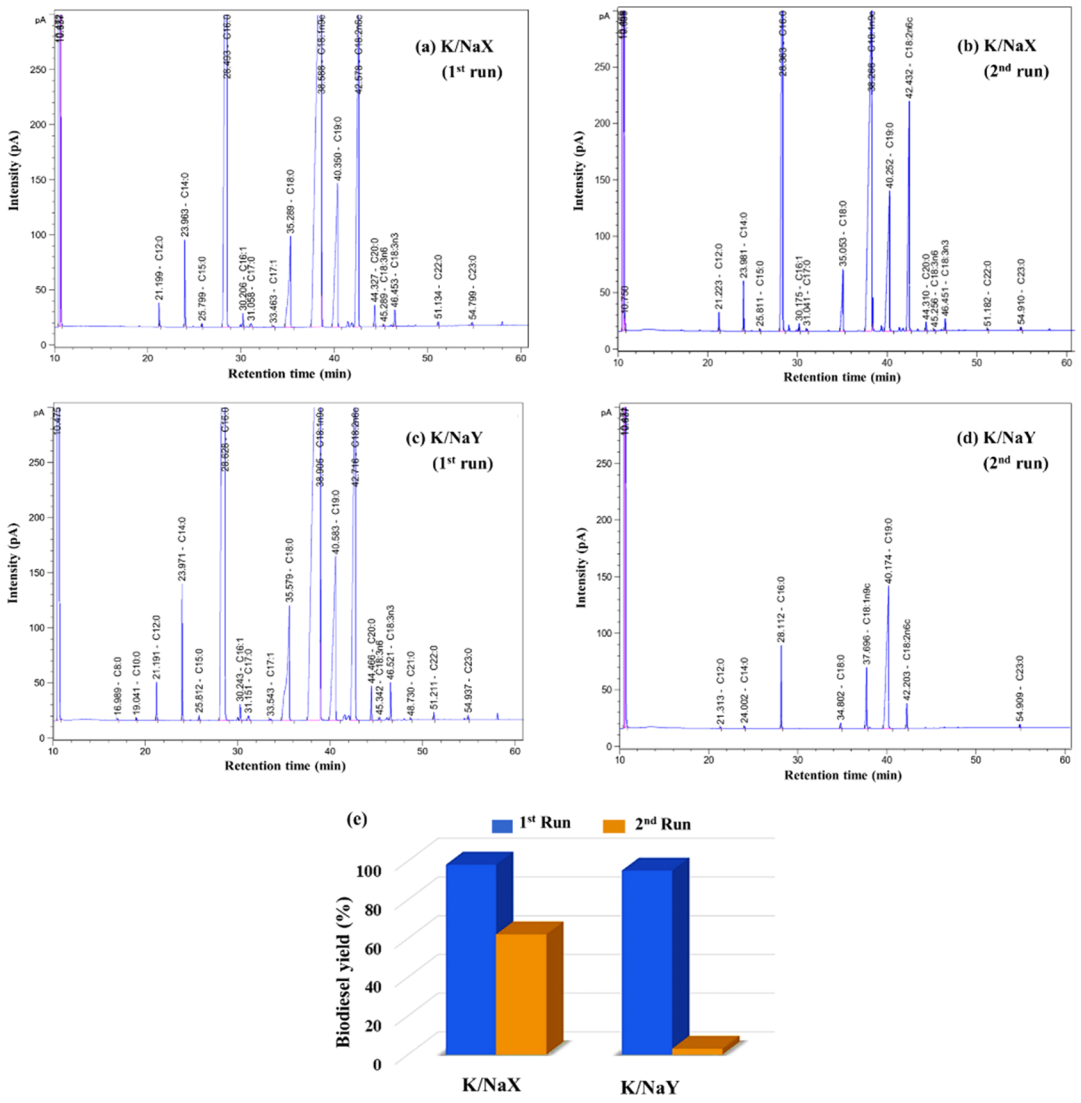

Figure 6. GC chromatograms of biodiesel products from the conversion of palm oil obtained from (a) K/NaX (1st run), (b) K/NaX (2nd run), (c) K/NaY (1st run), (d) K/NaY (2nd run), and (e) biodiesel yield from first and second run on K/NaX and K/NaY at 60 °C for 3 h.

Table 4. Comparison of the Catalyst Performance in Transesterification between K/NaX and K/NaY with 12 wt % K Loading from Conventional and Ultrasound-Assisted Impregnation from This Work and Literature

catalyst	preparation method	oil type	condition	biodiesel yield (mol %)	reference
K/NaX	impregnation	jatropha seed oil	65 °C, 3 h	83.0	17
K/NaY	impregnation	jatropha seed oil	65 °C, 3 h	73.4	13
K/NaY	impregnation	palm oil	60 °C, 3 h	68.6	12
K/NaY	ultrasound-assisted impregnation	palm oil	60 °C, 3 h	72.4	12
K/NaY	ultrasound-assisted impregnation	palm oil	60 °C, 3 h	94.4 ± 0.93	this work
K/NaX	ultrasound-assisted impregnation	palm oil	60 °C, 3 h	97.9 ± 0.52	this work

3. CONCLUSIONS

Potassium catalysts supported on FAU zeolites (K/NaX and K/NaY) were prepared using potassium acetate buffer through ultrasound-assisted impregnation. Calcination converts potassium precursor to potassium carbonate and causes the collapse of zeolite structures. The collapse in K/NaY is more than that in K/NaX. In addition, the basicity of K/NaX is higher than that of K/NaY.

In transesterification of palm oil and methanol, both catalysts provided high biodiesel yields in the first run. The yield decreased 1.6 times for K/NaX in the second run, but K/NaY was almost inactive. Possible causes of the lower performance of the catalysts are the leaching of potassium species, the collapse of the zeolite structure and the changes of the carbonate species. The effects are less pronounced on K/NaX; therefore, it is the better catalyst for this reaction. Further study to understand the interaction of potassium carbonate on the zeolite is recommended to design catalysts with high stability.

https://doi.org/10.1021/acsomega.1c04912
ACS Omega 2022, 7, 9130−9141

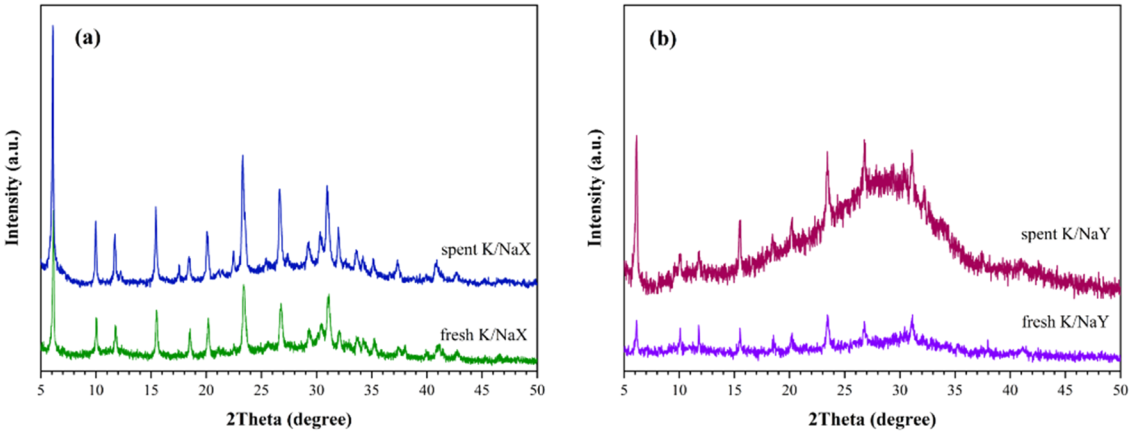

Figure 7. XRD patterns of (a) spent K/NaX and (b) spent K/NaY compared with fresh catalysts.

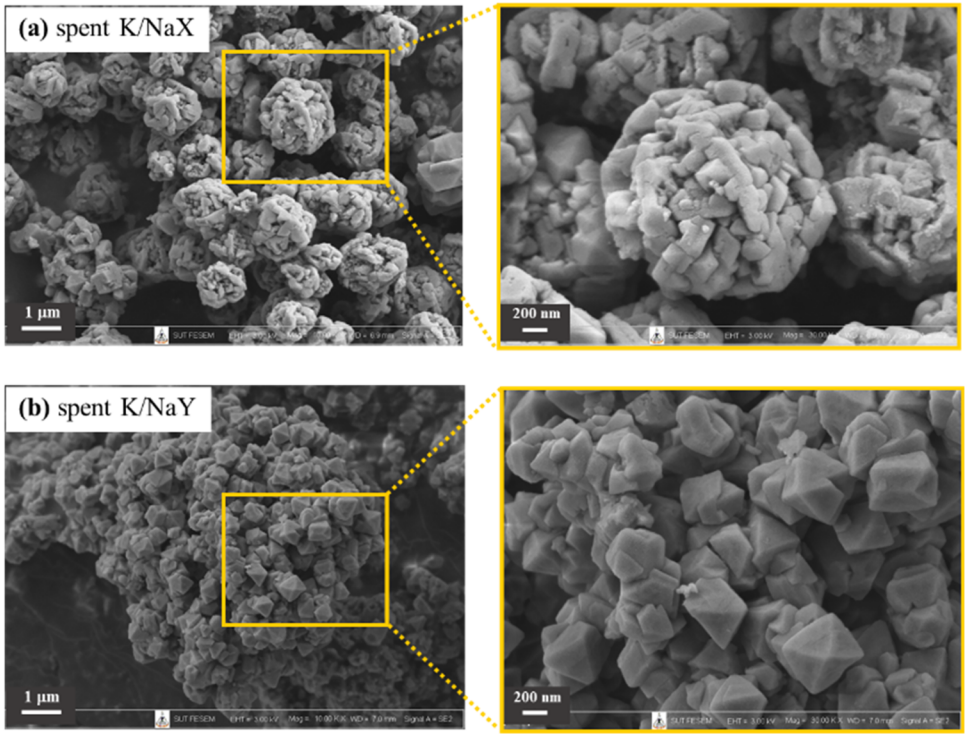

Figure 8. SEM images of (a) spent K/NaX and (b) spent K/NaY catalysts with 10k and 30k magnification.

4. MATERIALS AND METHODS

4.1. Catalyst Preparation. The synthesis methods of NaX (Si/Al = 1.2) and NaY (Si/Al = 2.4) as zeolite supports were modified from the literature.[41,42] Fumed silica (SiO_2, 99%, Sigma-Aldrich) was used as Si source for both zeolite syntheses. Aluminum trihydrate ($Al(OH)_3$, Panreac, 90%) and sodium aluminate ($NaAlO_2$, Al_2O_3 ~ 55−56%, Riedel-de Haën) were used as Al sources for the synthesis of NaX and NaY, respectively.

The catalysts with potassium loading of 12 wt % were prepared by ultrasound-assisted impregnation.[12] The zeolite supports were dried in a vacuum oven at 100 °C overnight. An acetate buffer was prepared by dissolving 5.70 g of potassium acetate (CH_3COOK, 99.0%, Carlo Erba) in 1.00 M acetic acid (CH_3COOH, 99.7%, RCI Labscan) and adjusted to 25.00 mL. The buffer of 1.20 mL was added to 1.00 g of dried zeolite and sonicated with frequency 37 kHz, power 80 W (Elmasonic E 30H model, Elma) for 10 min. The mixture was dried in a vacuum oven at 100 °C overnight and calcined at 480 °C under a static air atmosphere for 3 h. The obtained catalysts were notated K/NaY and K/NaX.

4.2. Catalyst Characterization. Phase characteristics of the catalysts were studied by X-ray diffraction (XRD) on a Bruker XRD-D8 Advance with Cu K_α radiation (λ = 0.154 nm) operated with a voltage of 40 kV and a current of 40 mA. All patterns were collected by a 2θ scan range from 5 to 50° with a step size of 0.02° at a scan speed of 0.5 s $step^{-1}$.

Isotherms of all samples were measured by N_2 adsorption−desorption using a BELSORP-mini II. These samples were degassed at 200 °C for 24 h. Surface areas were calculated by Brunauer−Emmett−Teller (BET) method and micropore volumes were estimated by *t*-plot method from the desorption branch.

Functional groups of samples were confirmed by Fourier transform infrared spectroscopy (FTIR) on a Bruker,

https://doi.org/10.1021/acsomega.1c04912
ACS Omega 2022, 7, 9130−9141

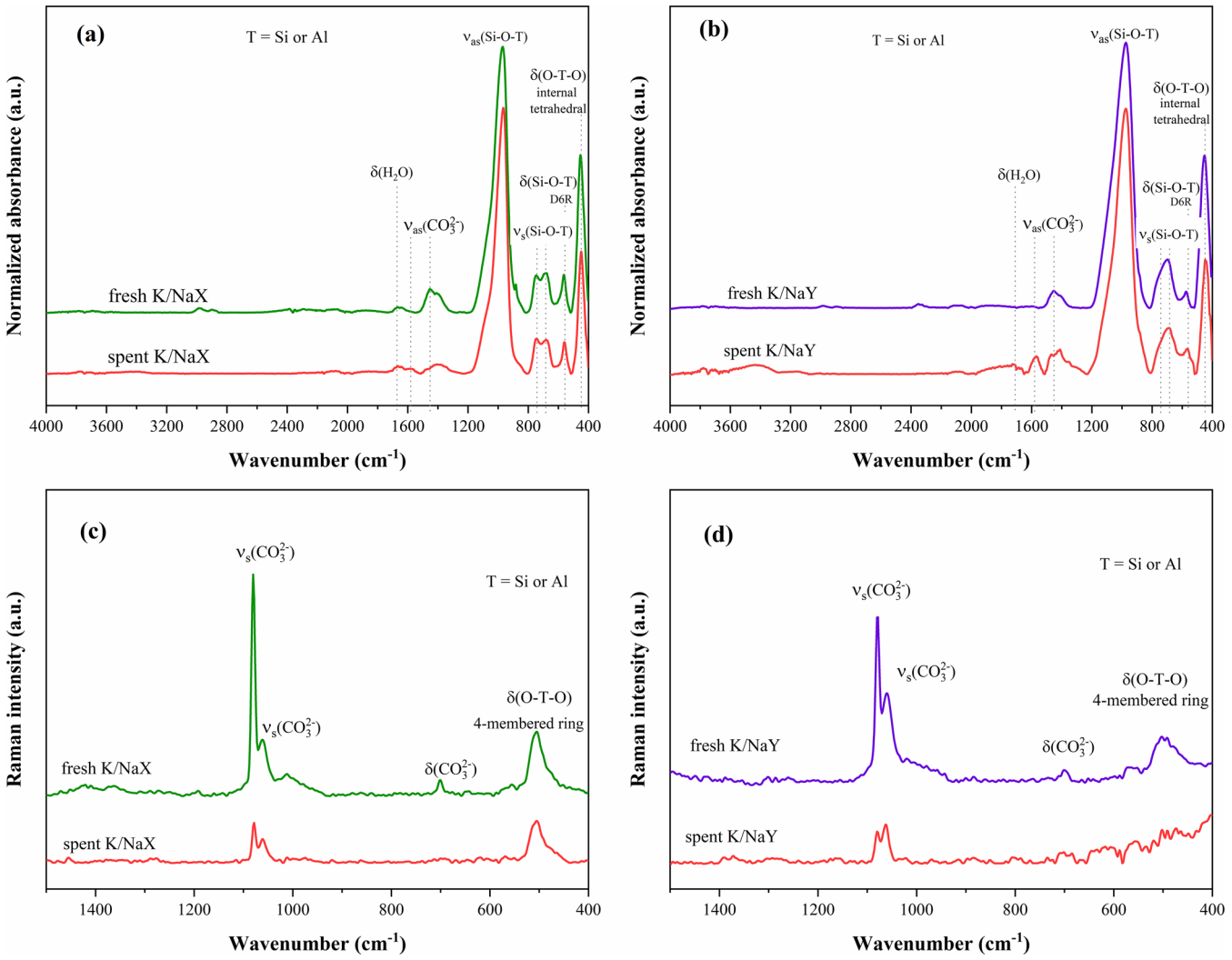

Figure 9. Comparison between fresh and spent catalysts by FTIR (ATR mode) spectra of (a) K/NaX and (b) K/NaY and Raman spectra of (c) K/NaX and (d) K/NaY.

Tensor27-Hyperion, spectrometer equipped with a microscope using the KBr pellet technique. The spectrum was recorded from 4000 to 400 cm^{-1} with a resolution of 4 cm^{-1} and 64 scans.

Raman spectra were collected with FT-Raman spectrometer on a Bruker, Vertex 70v-RAM II equipped with an Nd:YAG laser with an excitation wavelength of 1064 nm operated at a power of 300 mW. A signal was detected by a liquid nitrogen-cooled Ge diode. Each spectrum was recorded from 1500 to 50 cm^{-1} with 500 scans and a resolution of 4 cm^{-1}.

The Si/Al ratio of NaX and NaY and potassium content of the catalysts were determined by an inductive coupled plasma optical emission spectrometer (ICP-OES) using an Optima 8000 (PerkinElmer) instrument. Prior to measurement, the catalyst powder was digested using a microwave digestion method (Multiwave 3000 model, Anton Parr).

Both chemical surface species and surface interaction were identified by X-ray photoelectron spectroscopy (XPS) using a ULVAC-PHI PHI5000 VersaProbe II with Al K_α radiation. All binding energy (BE) peaks were calibrated corresponding to the standard C 1s peak at 284.6 eV. A Shirley background subtraction was applied to correct the XPS spectra stemming from inelastic electron scattering. XPS peaks were fitted with a combination of Gaussian (G) and Lorentzian (L) functions with a G to L ratio of 20 to 80. The full width at half-maximum (fwhm) of fitted peaks are in the range of 1.1−1.8 eV and 1.1−1.7 eV for C 1s and K 1s, respectively.

The basicity of the samples compared to the parent zeolites was studied by the decomposition of 2-methylbut-3-yn-2-ol (MBOH) in a fixed-bed reactor described in previous research.[43] A sample of 200 mg was loaded into a tubular stainless reactor and pretreated at 350 °C under a N_2 atmosphere. The reactor was then cooled down to 120 °C and flushed with a vaporized mixture of MBOH and toluene (95:5) using N_2 carrier gas with a flow rate of 10 mL min^{-1}. The conversion of MBOH and product selectivity were estimated according to equations reported in the literature.[44] The MBOH conversion and selectivity of decomposed products were calculated on the basis of the sum peak areas as follows in eqs 1 and 2, respectively.

$$\text{MBOH conversion(mol\%)} = \left(1 - \frac{A_{\text{MBOH}} rRF_{\text{MBOH}}/M_{\text{MBOH}}}{\sum_i (A_i rRF_i/M_i)}\right)100 \quad (1)$$

https://doi.org/10.1021/acsomega.1c04912
ACS Omega 2022, 7, 9130−9141

$$\text{product selectivity (mol\%)} = \frac{A_p \text{rRF}_p / M_p}{\sum (A_x \text{rRF}_x / M_x)} 100 \quad (2)$$

where peak area ratio (A), relative response factor (rRF), and molecular weight (M) are mathematical variables for all components i including MBOH and all products. The terms of the desired product and each obtained product are subscripted by p and x, respectively. The calculation method is based on the relative response factor defined by the effective carbon number concept (ECN).

The basicity of the catalysts was investigated by temperature-programmed desorption of carbon dioxide (CO_2-TPD) using a BELCAT-B chemisorption analyzer. A 50 mg sample was packed into a tubular glass reactor and pretreated at 300 °C under helium (He) gas flow with a rate of 50 mL min^{-1} for 60 min to eliminate physisorbed species. It was then cooled to 70 °C, and a gas mixture of 10% CO_2/He with a flow rate of 50 mL min^{-1} was introduced into the sample cell for 30 min. After that, it was purged with He for 30 min and heated to 100 °C with a rate of 10 °C min^{-1} and held for 60 min to remove nonadsorbed CO_2. The TPD process was performed in a temperature range of 100 to 800 °C with a temperature ramp of 10 °C min^{-1}. The basic site density was obtained by integration of the peak area.

4.3. Transesterification of Palm Oil. Transesterification of palm oil was performed according to the previous work.[12] Two-tenths of a gram of catalyst, 2.90 g of methanol (CH_3OH, 99.9%, Carlo Erba), and 5.00 g of refined palm oil (food grade, Morakot Industries PCL, Thailand) were stirred in a round-bottom flask equipped with a condenser at 60 °C for 3 h. The product mixture was separated by hot filtration following the literature.[45] The liquid phase was transferred to a separatory funnel and allowed to separate overnight. The produced biodiesel in the top layer was collected and evaporated to remove methanol using a rotary evaporator.

The quantitative content of methyl esters ($x_{\text{methyl esters}}$) was determined according to biodiesel test method EN 14103 by gas chromatography (Agilent 7890 GC) equipped with a flame ionization detector (FID) using a capillary column (Agilent J&W CP-Sil 88, CP7489) with a length of 100 m with a film thickness of 0.20 μm and an internal diameter of 0.25 mm. Helium was used as a carrier gas with a flow rate of 3 mL min^{-1}. The injection was performed in split mode with a split ratio of 50:1. The injector and detector temperatures were 240 and 300 °C, respectively. In the first step, the oven temperature was started at 70 °C for 4 min and heated to 175 °C with a ramp rate of 13 °C min^{-1} and held for 27 min. In the second step, the oven was heated to 215 °C with a ramp rate of 4 °C min^{-1} and kept for 15 min. In the final step, the oven temperature was increased to 240 °C with a ramp rate of 4 °C min^{-1} and kept for 12 min. Methyl nonadecanoate, so-called $C_{19}(CH_3(CH_2)_{17}COOCH_3$, 98%, Sigma-Aldrich) was used as the internal standard. The content of methyl esters from the received biodiesel was obtained from eq 3, whereas the content of triglycerides ($x_{\text{triglycerides}}$) was from the literature.[46] The yield of produced biodiesel was calculated according to eq 4 from the literature.[47]

$$x_{\text{methyl esters}} = \left(\frac{(\Sigma A_{C_{14}-C_{24:1}}) - A_{C_{19}}}{A_{C_{19}}}\right)\left(\frac{[C_{19}]V_{C_{19}}}{m_{\text{sample}}}\right)100 \quad (3)$$

where $\Sigma A_{C_{14}\text{-}C_{24:1}}$ is the total peak area from methyl ester in C_{14} to that in $C_{24:1}$ obtained from GC-FID, and m_{sample} is the mass of the analyzed biodiesel sample. The GC peak area, concentration, and volume of methyl nonadecanoate solution are represented by A_{C19}, $[C_{19}]$, and V_{C19}, respectively.

$$\text{biodiesel yield (mol\%)} = \left(\frac{m_{\text{biodiesel}}}{m_{\text{palm oil}}}\right)\left(\frac{x_{\text{methyl esters}}}{x_{\text{triglycerides}}}\right)\left(\frac{M_{\text{triglycerides}}}{3M_{\text{methyl esters}}}\right)100 \quad (4)$$

where $m_{\text{biodiesel}}$ and $m_{\text{palm oil}}$ are the mass of biodiesel and palm oil. $M_{\text{methyl esters}}$ and $M_{\text{triglycerides}}$ are average molecular weight of methyl ester or triglyceride (as indicated with a subscript), whereas number 3 is the stoichiometric coefficient from the balanced chemical equation of transesterification of triglycerides with methanol.

The catalyst stability was investigated by reusing the spent catalysts and characterization by XRD, SEM, and FTIR with attenuated total reflection (ATR), and Raman spectroscopy. The spent catalysts were washed with methanol (10 mL) and hexane (5 mL) and dried at 90 °C overnight. The potassium leaching was determined by ICP-OES. The K content from separated liquid products including biodiesel and glycerol was determined. Each liquid product was digested by a microwave digestion method (Multiwave 3000 model, Anton Parr). The percentage of K leaching was calculated according to Čapek et al.[40]

AUTHOR INFORMATION

Corresponding Author

Jatuporn Wittayakun − *School of Chemistry, Institute of Science, Suranaree University of Technology, Nakhon Ratchasima 30000, Thailand;* orcid.org/0000-0002-4426-2825; Email: jatuporn@sut.ac.th

Authors

Siriporn Kosawatthanakun − *School of Chemistry, Institute of Science, Suranaree University of Technology, Nakhon Ratchasima 30000, Thailand*

Chaianun Pansakdanon − *School of Chemistry, Institute of Science, Suranaree University of Technology, Nakhon Ratchasima 30000, Thailand*

Narongrit Sosa − *National Nanotechnology Center (NANOTEC), National Science and Technology Development Agency (NSTDA), Pathum, Thani 12120, Thailand;* orcid.org/0000-0002-7745-329X

Narong Chanlek − *Synchrotron Light Research Institute (Public Organization), Nakhon, Ratchasima 30000, Thailand*

Frank Roessner − *Industrial Chemistry 2, Institute of Pure and Applied Chemistry, Carl von Ossietzky University of Oldenburg, Oldenburg D-26111, Germany;* orcid.org/0000-0003-2455-0579

Sanchai Prayoonpokarach − *School of Chemistry, Institute of Science, Suranaree University of Technology, Nakhon Ratchasima 30000, Thailand*

Complete contact information is available at: https://pubs.acs.org/10.1021/acsomega.1c04912

Notes

The authors declare no competing financial interest.

https://doi.org/10.1021/acsomega.1c04912
ACS Omega 2022, 7, 9130−9141

■ ACKNOWLEDGMENTS

S.K. is supported by the Royal Golden Jubilee Ph.D. Program (Grant PHD/0142/2557) from the Thailand Research Fund (TRF) and Thai German S&T Cooperation 3rd Researcher Mobility. The scholarship for C.P. is from the Science Achievement Scholarship of Thailand.

■ REFERENCES

(1) Refaat, A. A. Biodiesel production using solid metal oxide catalysts. *Int. J. Environ. Sci. Technol.* **2011**, *8* (1), 203−221.
(2) Romero, M. D.; Ovejero, G.; Rodríguez, A.; Gómez, J. M. Enhancement of the basic properties in FAU zeolites by impregnation with cesium hydroxide. *Microporous Mesoporous Mater.* **2005**, *81* (1−3), 313−320.
(3) Perego, C.; Bosetti, A.; Ricci, M.; Millini, R. Zeolite materials for biomass conversion to biofuel. *Energy Fuels* **2017**, *31* (8), 7721−7733.
(4) Muciño, G. E. G.; Romero, R.; García-Orozco, I.; Serrano, A. R.; Jiménez, R. B.; Natividad, R. Deactivation study of K_2O/NaX and Na_2O/NaX catalysts for biodiesel production. *Catal. Today* **2016**, *271*, 220−226.
(5) Mukhtar, A.; Saqib, S.; Lin, H.; Hassan Shah, M. U.; Ullah, S.; Younas, M.; Rezakazemi, M.; Ibrahim, M.; Mahmood, A.; Asif, S.; Bokhari, A. Current status and challenges in the heterogeneous catalysis for biodiesel production. *Renew. Sust. Energy Rev.* **2022**, *157*, 112012.
(6) Mathew, G. M.; Raina, D.; Narisetty, V.; Kumar, V.; Saran, S.; Pugazhendi, A.; Sindhu, R.; Pandey, A.; Binod, P. Recent advances in biodiesel production: Challenges and solutions. *Sci. Total Environ.* **2021**, *794*, 148751.
(7) Mohiddin, M. N. B.; Tan, Y. H.; Seow, Y. X.; Kansedo, J.; Mubarak, N. M.; Abdullah, M. O.; Chan, Y. S.; Khalid, M. Evaluation on feedstock, technologies, catalyst and reactor for sustainable biodiesel production: A review. *J. Ind. Eng. Chem.* **2021**, *98*, 60−81.
(8) Ganesan, R.; Manigandan, S.; Shanmugam, S.; Chandramohan, V. P.; Sindhu, R.; Kim, S.-H.; Brindhadevi, K.; Pugazhendhi, A. A detailed scrutinize on panorama of catalysts in biodiesel synthesis. *Sci. Total Environ.* **2021**, *777*, 145683.
(9) Okolie, J. A.; Ivan Escobar, J.; Umenweke, G.; Khanday, W.; Okoye, P. U. Continuous biodiesel production: A review of advances in catalysis, microfluidic and cavitation reactors. *Fuel* **2022**, *307*, 121821.
(10) Bashir, M. A.; Wu, S.; Zhu, J.; Krosuri, A.; Khan, M. U.; Ndeddy Aka, R. J. Recent development of advanced processing technologies for biodiesel production: A critical review. *Fuel Process. Technol.* **2022**, *227*, 107120.
(11) Hindryawati, N.; Maniam, G. P.; Karim, M. R.; Chong, K. F. Transesterification of used cooking oil over alkali metal (Li, Na, K) supported rice husk silica as potential solid base catalyst. *Eng. Sci. Technol. Int. J.* **2014**, *17* (2), 95−103.
(12) Rakmae, S.; Keawkumay, C.; Osakoo, N.; Montalbo, K. D.; de Leon, R. L.; Kidkhunthod, P.; Chanlek, N.; Roessner, F.; Prayoonpokarach, S.; Wittayakun, J. Realization of active species in potassium catalysts on zeolite NaY prepared by ultrasound-assisted impregnation with acetate buffer and improved performance in transesterification of palm oil. *Fuel* **2016**, *184*, 512−517.
(13) Supamathanon, N.; Wittayakun, J.; Prayoonpokarach, S. Properties of Jatropha seed oil from Northeastern Thailand and its transesterification catalyzed by potassium supported on NaY zeolite. *J. Ind. Eng. Chem.* **2011**, *17* (2), 182−185.
(14) Verboekend, D.; Nuttens, N.; Locus, R.; Van Aelst, J.; Verolme, P.; Groen, J. C.; Pérez-Ramírez, J.; Sels, B. F. Synthesis, characterisation, and catalytic evaluation of hierarchical faujasite zeolites: milestones, challenges, and future directions. *Chem. Soc. Rev.* **2016**, *45* (12), 3331−3352.
(15) Polisi, M.; Grand, J.; Arletti, R.; Barrier, N.; Komaty, S.; Zaarour, M.; Mintova, S.; Vezzalini, G. CO_2 adsorption/aesorption in FAU zeolite nanocrystals: in situ synchrotron X-ray powder diffraction and in situ Fourier transform infrared spectroscopic study. *J. Phys. Chem. C* **2019**, *123* (4), 2361−2369.
(16) Zito, P. F.; Caravella, A.; Brunetti, A.; Drioli, E.; Barbieri, G. Estimation of Langmuir and Sips Models adsorption parameters for NaX and NaY FAU zeolites. *J. Chem. Eng. Data* **2015**, *60* (10), 2858−2868.
(17) Manadee, S.; Sophiphun, O.; Osakoo, N.; Supamathanon, N.; Kidkhunthod, P.; Chanlek, N.; Wittayakun, J.; Prayoonpokarach, S. Identification of potassium phase in catalysts supported on zeolite NaX and performance in transesterification of Jatropha seed oil. *Fuel Process. Technol.* **2017**, *156*, 62−67.
(18) Noiroj, K.; Intarapong, P.; Luengnaruemitchai, A.; Jai-In, S. A comparative study of KOH/Al_2O_3 and KOH/NaY catalysts for biodiesel production via transesterification from palm oil. *Renew. Energy* **2009**, *34* (4), 1145−1150.
(19) Peña, R.; Romero, R.; Martínez, S. L.; Natividad, R.; Ramírez, A. Characterization of KNO_3/NaX catalyst for sunflower oil transesterification. *Fuel* **2013**, *110*, 63−69.
(20) Intarapong, P.; Luengnaruemitchai, A.; Jai-In, S. Transesterification of palm oil over KOH/NaY zeolite in a packed-bed reactor. *Int. J. Renew. Energy Res.* **2011**, *1* (4), 271−280.
(21) Xie, W.; Huang, X.; Li, H. Soybean oil methyl esters preparation using NaX zeolites loaded with KOH as a heterogeneous catalyst. *Bioresour. Technol.* **2007**, *98* (4), 936−939.
(22) Montalbo, K. D.; Leon, R. L. d.; Sophiphun, O.; Manadee, S.; Prayoonpokarach, S.; Wittayakun, J. Characterization and catalytic performance of potassium loaded on rice husk silica and zeolite nay for transesterification of jatropha seed oil. *Quim. Nova* **2013**, *36*, 1116−1120.
(23) Sosa, N.; Chanlek, N.; Wittayakun, J. Facile ultrasound-assisted grafting of silica gel by aminopropyltriethoxysilane for aldol condensation of furfural and acetone. *Ultrason. Sonochem.* **2020**, *62*, 104857.
(24) Ketzer, F.; Celante, D.; de Castilhos, F. Catalytic performance and ultrasonic-assisted impregnation effects on WO_3/USY zeolites in esterification of oleic acid with methyl acetate. *Microporous Mesoporous Mater.* **2020**, *291*, 109704.
(25) Thommes, M.; Kaneko, K.; Neimark, A. V.; Olivier, J. P.; Rodriguez-Reinoso, F.; Rouquerol, J.; Sing, K. S.W. Physisorption of gases, with special reference to the evaluation of surface area and pore size distribution (IUPAC Technical Report). *Pure Appl. Chem.* **2015**, *87* (9−10), 1051−1069.
(26) Lavalley, J. C. Infrared spectrometric studies of the surface basicity of metal oxides and zeolites using adsorbed probe molecules. *Catal. Today* **1996**, *27* (3), 377−401.
(27) Binet, C.; Daturi, M.; Lavalley, J.-C. IR study of polycrystalline ceria properties in oxidised and reduced states. *Catal. Today* **1999**, *50* (2), 207−225.
(28) Edwards, H. G. M.; Villar, S. E. J.; Jehlicka, J.; Munshi, T. FT-Raman spectroscopic study of calcium-rich and magnesium-rich carbonate minerals. *Spectrochim. Acta A Mol. Biomol. Spectrosc.* **2005**, *61* (10), 2273−2280.
(29) Frantz, J. D. Raman spectra of potassium carbonate and bicarbonate aqueous fluids at elevated temperatures and pressures: comparison with theoretical simulations. *Chem. Geol.* **1998**, *152* (3), 211−225.
(30) Ishimaru, Y.; Oshima, Y.; Imai, Y.; Iimura, T.; Takanezawa, S.; Hino, K.; Miura, H. Raman spectroscopic analysis to detect reduced bone quality after sciatic neurectomy in mice. *Molecules* **2018**, *23* (12), 3081.
(31) Swathy, J. R.; Pugazhenthiran, N.; Sudhakar, C.; Anil Kumar, A.; Pradeep, T. Sparingly Soluble Constant Carbonate Releasing Inert Monolith for Enhancement of Antimicrobial Silver Action and Sustainable Utilization. *ACS Sustain. Chem. Eng.* **2016**, *4* (7), 4043−4049.
(32) Sun, P.; Yu, D.; Tang, Z.; Li, H.; Huang, H. NaY zeolites catalyze dehydration of lactic acid to acrylic acid: studies on the effects of anions in potassium salts. *Ind. Eng. Chem. Res.* **2010**, *49* (19), 9082−9087.

https://doi.org/10.1021/acsomega.1c04912
ACS Omega 2022, 7, 9130−9141

(33) Lauron-Pernot, H.; Luck, F.; Popa, J. M. Methylbutynol: a new and simple diagnostic tool for acidic and basic sites of solids. *Appl. Catal.* **1991**, *78* (2), 213−225.
(34) Ma, Y.-K.; Rigolet, S.; Michelin, L.; Paillaud, J.-L.; Mintova, S.; Khoerunnisa, F.; Daou, T. J.; Ng, E.-P. Facile and fast determination of Si/Al ratio of zeolites using FTIR spectroscopy technique. *Microporous Mesoporous Mater.* **2021**, *311*, 110683.
(35) Mozgawa, W. The relation between structure and vibrational spectra of natural zeolites. *J. Mol. Struct.* **2001**, *596* (1), 129−137.
(36) Abu-Zied, B. M. Cu^{2+}-acetate exchanged X zeolites: Preparation, characterization and N_2O decomposition activity. *Microporous Mesoporous Mater.* **2011**, *139* (1−3), 59−66.
(37) Phung, T. K.; Carnasciali, M. M.; Finocchio, E.; Busca, G. Catalytic conversion of ethyl acetate over faujasite zeolites. *Appl. Catal. A Gen.* **2014**, *470*, 72−80.
(38) Zhong, X.-H.; Liu, Y.; Xu, T.; Liu, W.-Y. Influencing factors of intercalation of potassium acetate into dickite using immersion method. *J. Alloys Compd.* **2018**, *742*, 996−1001.
(39) Fan, M.; Zhang, P.; Zhang, Y. NaY zeolite-supported potassium salt catalysts for dipropyl carbonate synthesis from transesterification route. *Chem. Eng. Commun.* **2011**, *198* (8), 1033−1040.
(40) Čapek, L.; Hájek, M.; Kutálek, P.; Smoláková, L. Aspects of potassium leaching in the heterogeneously catalyzed transesterification of rapeseed oil. *Fuel* **2014**, *115*, 443−451.
(41) Lechert, H.; Staelin, P., Linde Type X. In *Verified Syntheses of Zeolitic Materials*, third ed.; Mintova, S., Ed.; The Synthesis Commission of the International Zeolite Association, 2016; pp 215−217.
(42) Ginter, D., Linde Type Y. In *Verified syntheses of Zeolitic Materials*, third ed.; Mintova, S., Ed.; The Synthesis Commission of the International Zeolite Association, 2016; pp 221−223.
(43) Novikova, L.; Roessner, F.; Belchinskaya, L.; AlSawalha, M.; Krupskaya, V. Study of surface acid−base properties of natural clays and zeolites by the conversion of 2-methylbut-3-yn-2-ol. *Appl. Clay Sci.* **2014**, *101*, 229−236.
(44) Supamathanon, S.; Wittayakun, J.; Prayoonpokarach, S.; Supronowicz, W.; Roessner, F. Basic properties of potassium oxide supported on zeolite Y studied by Pyrrole-TPD and catalytic conversion of methylbutynol. *Quim. Nova* **2012**, *35* (9), 1719−1723.
(45) Sheldon, R. A.; Wallau, M.; Arends, I. W. C. E.; Schuchardt, U. Heterogeneous catalysts for liquid-phase oxidations: Philosophers' Stones or Trojan Horses? *Acc. Chem. Res.* **1998**, *31*, 485−493.
(46) Roschat, W.; Siritanon, T.; Yoosuk, B.; Promarak, V. Biodiesel production from palm oil using hydrated lime-derived CaO as a low-cost basic heterogeneous catalyst. *Energy Convers. Manag.* **2016**, *108*, 459−467.
(47) Okwundu, O. S.; El-Shazly, A. H.; Elkady, M. Comparative effect of reaction time on biodiesel production from low free fatty acid beef tallow: a definition of product yield. *SN Appl. Sci.* **2019**, *1* (2), 140.

https://doi.org/10.1021/acsomega.1c04912
ACS Omega 2022, 7, 9130−9141